

Using machine learning to observe and understand microwave induced steps in the IV of a superconducting quantum interference device

L. Bult, N. Verhoecks, B. Wagemakers*

Applied Physics, Delft University of Technology, Lorentzweg 1, 2628 CJ Delft.

(Dated: January 20, 2022)

Shapiro steps can be found in an IV-curve when microwaves are transmitted to a Mr. Squid probe lowered in liquid nitrogen. This report describes how to use machine learning to observe and understand these Shapiro steps, how to use machine learning to find the combinations of RF power and frequency automatically and if there are any consistent differences in frequency and or power where (Shapiro) steps can be found.

In the experiment a Mr SQUID probe is lowered into a dewar with liquid nitrogen and when the probe is superconducting, a microwave generator is turned on. IV-curves of the probe are subsequently plotted using Mr SQUID's data. Multiple neural networks were then trained using a selection of all gathered data. This is done by using the Scikit-Learn Python library function "MLPClassifier".

The machine learning method has successfully demonstrated that it is capable of selecting IV-curves similar to the ones in the training set. Those IV-curves were found to occur at different RF power for varying frequency. It was thought that interference of the electromagnetic waves might be the reason for the variation in RF power at frequencies at which step curves were found.

Periodicity of observed steps consistent with theoretically predicted Shapiro steps has been demonstrated at four frequencies. Constant voltage occurrence of steps at varying power has also been demonstrated. Additionally, Shapiro step candidates were visible on every sampled frequency to date. It must be noted that the test size is too small for a statistically significant conclusion. Therefore, the authors come to the conclusion that although there is some evidence to support the observation of Shapiro steps, it is left to future experimentation to confirm this observation.

I. INTRODUCTION

When two superconducting pieces are really close to each other the wave functions of the two pieces will overlap at the gap, if the gap is small enough the two pieces will act like a single one, this connection is called a Josephson junction. If one is sweeping out an IV-curve while applying an AC electric field to the Josephson junction, a curve with constant voltage steps in the IV-curve is visible. These steps are called Shapiro steps.

In this experiment a setup is build to transmit microwaves to a Mr. Squid probe lowered in liquid nitrogen. The goal of the experiment is using machine learning to observe and understand microwave induced steps in the IV-curve of a SQUID (superconducting quantum interference device). Other related questions to this experiment are: is there a faster way to find the Shapiro steps than manually changing the frequency of the microwaves? Is there a consistent difference in frequency and or power where the Shapiro steps can be found?

This report consists six chapters. The theory that is needed to understand the experiment is written out in chapter II. Chapter III describes the experimental method that is used for this experiment. Chapter IV describes the machine learning method. The results and discussions are split in two parts with one being dedicated to the machine learning approach and the other

being about the resulting steps, Chapter V and VI respectively. Chapter VII is the final chapter and it contains the conclusion.

II. THEORY

Superconducting charge carriers are described by a quantum wave function with an amplitude and a quantum phase. In a single piece of superconductor, the phases at two different positions have a specific relation to one another (macroscopic phase coherence). This arrangement assures a lower energy ground state that results in superconductivity. As quantum mechanics predicts the wave functions slightly extend into the outside region with an exponential decay. Thus, the wave functions of the two pieces will overlap at the gap, so if the gap region is small enough, they will be related. So the two superconductors will essentially act like a single one, but with a small region where the ability to carry a super current is reduced. Still, electrical currents can flow between the two regions with zero electrical resistance. Such tunnel currents are called Josephson currents and superconductors connected by this link are called Josephson junctions. Strictly speaking, the resistance-less currents that flow in a Josephson junction are a manifestation of the DC (direct current) Josephson effect; a second property of Josephson junctions by which the Cooper pair current oscillates with high frequencies through the gap is called the AC (alternating current) Josephson effect.

The current density (J) of a Josephson junction with a

* l.e.bult@student.tudelft.nl, n.l.verhoecks@student.tudelft.nl,
b.b.wagemakers@student.tudelft.nl

variable (oscillating) voltage (V) is given by the equation:

$$V(t) = V_0 + V_a \cos(\omega_u t) \quad (1)$$

then:

$$\begin{aligned} J(t) &= J_0 \sum_{n=1}^{\infty} (-1)^n J_n \left(\frac{4\pi e V_a}{h \omega_e} \right) \\ &\sin \left[\delta'(0) + \left(n \omega_a - \left(\frac{4\pi e V_0}{h} \right) \right) \right] \end{aligned} \quad (2)$$

This shows that when

$$V_0 = \frac{n h w_n}{4\pi e} \quad (3)$$

a discontinuous shift in the current with no change in the dc voltage across the junction occurs. Formula's 1 up and including 3 can be found in [1], including a more detailed derivation. If one is sweeping out a IV-curve while applying an AC electric field to the Josephson junction, one will see a curve similar to the one that appears below (Figure 1). Such constant voltage steps (i.e. discontinuous shift in the DC current) in the IV-curve are called Shapiro steps. In this report, "bias current" will be shortened to "current" in the graph axis labels.

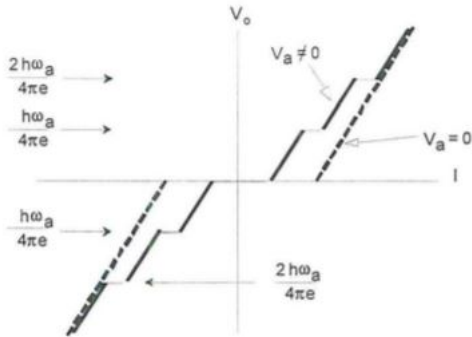


FIG. 1. Theoretical depiction of Shapiro steps in the IV curve of a Josephson Junction [1].

There are a number of ways to impress an AC voltage on Josephson Junctions (JJ's)[2]. The easiest way is to simply transmit the microwaves into the cryogenic container holding the JJ. Due to the high sensitivity of the JJ's, even at very modest RF power levels a significant amount of radiation will couple into the junctions despite the large impedance mismatch between the junctions and free space. Previously observed Shapiro steps, that are also expected to occur in this experiment, are shown in Figures 2 and 3. [3]

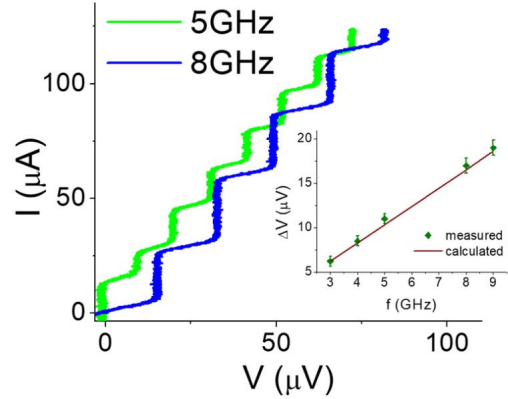


FIG. 2. Shapiro steps IV-curve as observed by [4].

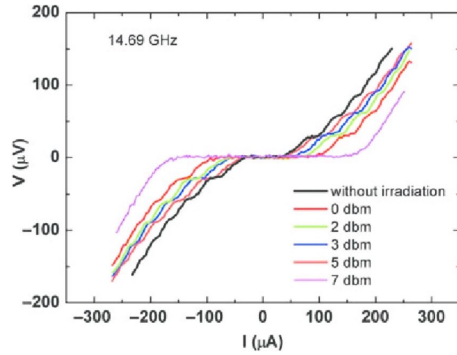


FIG. 3. Shapiro steps IV-curve evolution at a constant frequency of 14.69 GHz and a varying RF power (in dBm) [5].

III. METHOD: EXPERIMENTATION

A. Experimental Setup

The setup for this experiment consisted of various components being a superconducting quantum interference probe (Mr. Squid probe), a superconducting probe control box (Mr. Squid control box), an RF applications control board (Red Pitaya), an RF signal generator (Windfreak SynthNV PRO), a dewar with cryogenic liquid, magnetic shielding (aluminum foil) and a desktop PC with custom python measurement and data collection software. For more information (such as datasheets and applications) about the two main components, namely the superconducting probe and the RF signal generator one can use the following resources. For the probe it can be found at [6] and for the RF signal generator at [7]. To visualize the data from the probe, IV curves were used. The data from these curves was then saved and processed in order to find steps. The experimental setup was constructed as follows. At one end the RF control board was connected to the PC and at the other end to the probe control box. The RF signal generator was hooked up to a USB hub. This can be seen in Figures 4 and 5.

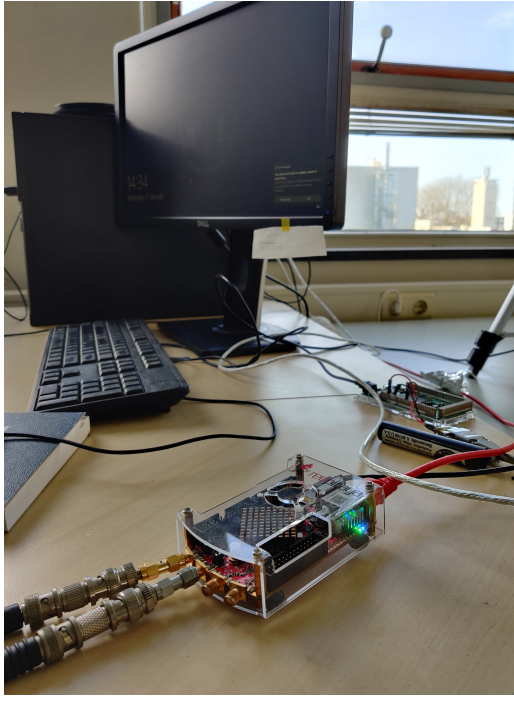


FIG. 4. The RF control board and project PC.

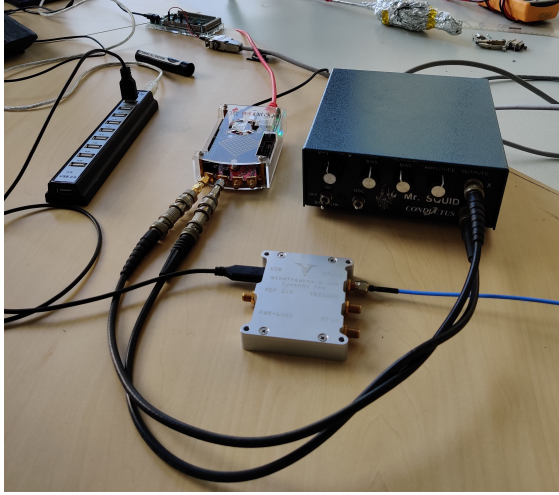


FIG. 5. Control Board, control box and RF signal generator.

The superconducting probe was connected to the probe control box. The RF signal generator had an antenna which was adhered to the probe with electrical tape. Both the probe and the antenna were wrapped in aluminum foil for magnetic shielding. The probe was connected to a long metal tube through which its signal cables ran. Pictures of the probe and antenna without the magnetic shielding can be seen in Figure 6, it also shows the exact position of the RF signal antenna endpoint. The probe with magnetic shielding and the metal tube with the signal cable connections can be seen in Figure 7, these run all the way to the probe control box.

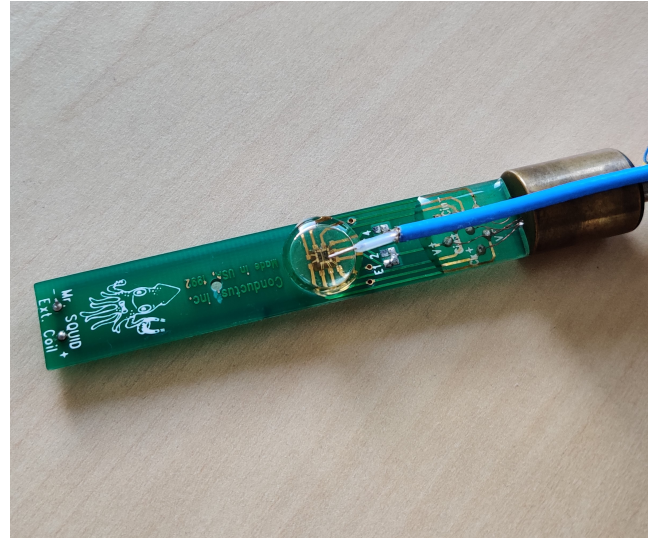


FIG. 6. The superconducting probe with the blue RF signal antenna without the magnetic shielding.



FIG. 7. Superconducting probe with magnetic shielding and cable connections.

In order to keep the probe in position in the dewar a custom adjustable stand was used. The metal tube was clamped in this stand so that it could be lowered in the dewar. Figures 8 and 9 show a schematic view of the probe in the dewar, and the setup in real life respectively. The part that is expected to induce the steps is the RF signal generator. Therefore, it deserves a separate section in order to elaborate on its specifications.

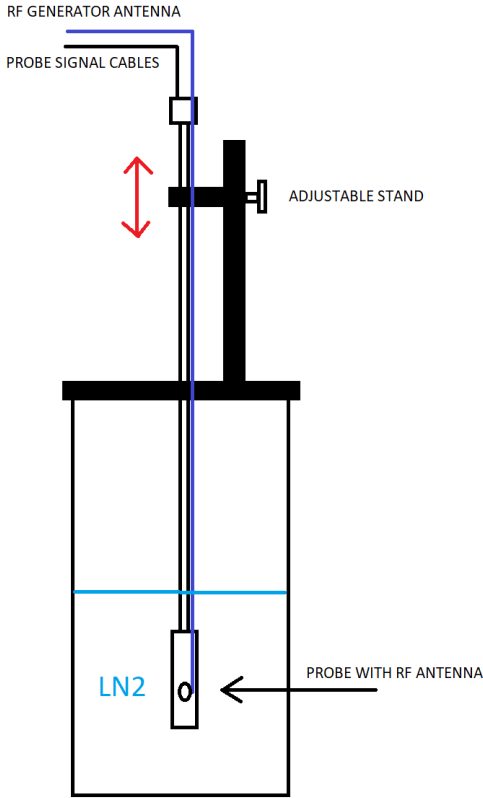


FIG. 8. Schematic view of the dewar with the probe fully submerged in LN2

B. The RF signal generator

The RF signal generator model that was used is a Windfreak SynthNV PRO with a frequency range of 12.5 MHz to 6.4 GHz, and a power level range of 50 dBm. The RF signal can be altered using dedicated software or Python. It can also be used as an RF signal detector with the same frequency and power range as the generator. The RF generator side has a multi band agile switching low pass filter for attenuating output harmonics. The SynthNV PRO can also be programmed to start by itself on any frequency, power, sweep or modulation setting (in any combination). In this way it can be used as portable RF signal generator/detector. The device accomplishes Scalar Network Analysis for both through and reflected (requires external 3rd party directional coupler) responses of RF devices such as filters, amplifiers, antennas, cavities, and matching networks. Frequency set to RFout – then measure RFin sweeps run at 150 μ s per point. Notably, the SynthNV PRO also has a 16 band high-speed switching harmonic filter on its output that attenuates harmonics up to 60 dBc.[7] Figure 10 shows a 3D view of the device in which all the ports and connectors with description are visible.

The RF output performance for a range of 500 to 6400 MHz can be seen in Figure 11 and typical calibra-



FIG. 9. The dewar with LN2 and the probe with its probe stand. At this point the probe is fully submerged.

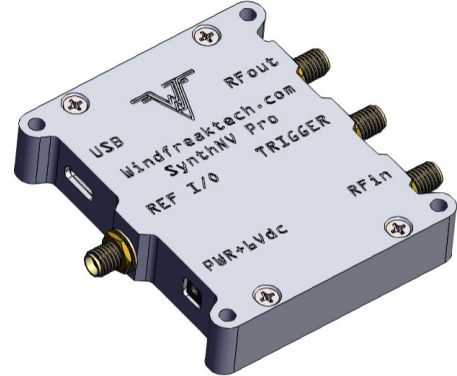


FIG. 10. 3D view of the Windfreak SynthNV PRO. Image courtesy of Windfreak technologies LLC [7].

tion for the output power can be found in Figure 12.

C. Measurements

In order to visualize the steps a Python program (courtesy of Prof. Steele) was used [8]. This program was tweaked to display an IV-curve of the Mr. Squid probe's current and voltage output. The RF generator can produce different frequencies at different power levels. The Python program was used to display an IV-curve for



FIG. 11. Max and Min power lines of the SynthNV in the range of 500 to 6400 MHz. The graph shows the power versus the frequency [7].

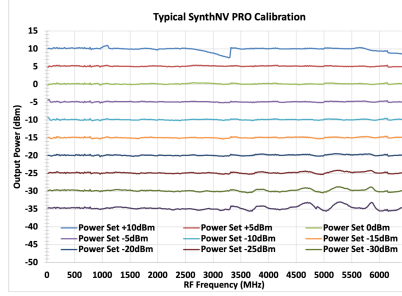


FIG. 12. Typical calibration of the SynthNV, the graphs show the output power against the frequency [7].

many combinations of frequency and power level. The range of the power levels and frequencies were -50 to 0 dBm and 1000 to 5000 MHz respectively. For the power levels steps of 1 dBm were used and for the frequencies it was steps of 10 MHz. The data from the IV graphs was then saved, after which it was formatted in order to be processed by the machine learning algorithm. An example of a typical IV-curve can be seen in Figure 13.

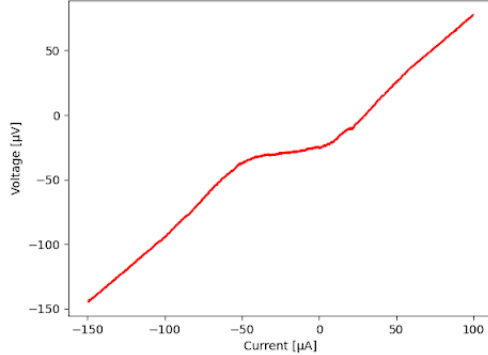


FIG. 13. Typical IV-curve produced by the Python software.

IV. METHOD: MACHINE LEARNING

A. Neural Network Filtering Architecture: Steps

Manual selection of (Shapiro) steps IV-curves is a tedious and time consuming process. The authors therefore devised a machine learning method to extract relevant data. Data is selected using two deep neural networks (DNN's). These neural networks are made and trained using the Scikit-Learn Python library function "MLPClassifier" [9]. Unfortunately, inference was not possible on the project PC, making it necessary to first collect data, and subsequently filter on a different computer. Although it is known that some graphs are incorrectly filtered (i.e. false negatives), the overall performance is satisfactory. Two DNN's were used for filtering the data. The architecture of the first DNN can be seen in Figure 14, this DNN will from now on be referred to as DNN1. This DNN takes as input 5000 raw voltage points and outputs; 0 if steps were detected, and 1 if no steps were detected. As can be seen in the figure, the input points are fed forward through 1000 neurons in the hidden layer. Although the neural network scored quite well on the training and verification set (see Table I in Section IV C), the authors think that it is not yet optimal and there is much to improve on (see Section V B).

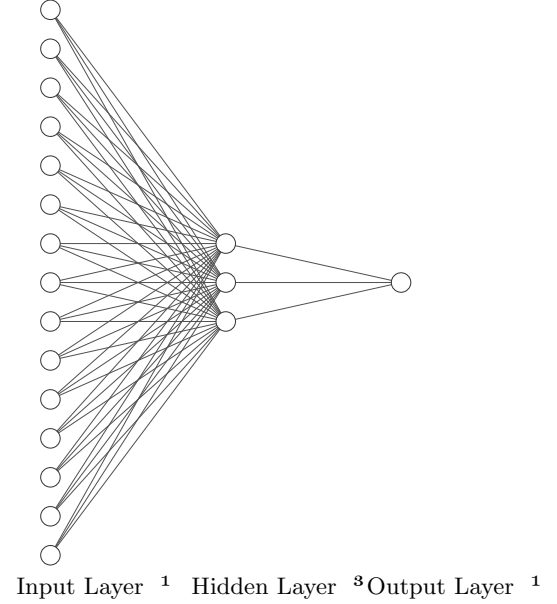


FIG. 14. Schematic of the raw IV curve deep neural network architecture. The ratio of the input-to-hidden layer neurons is 5:1, with 5000 inputs. The output layers consists of one neuron. Created using [10].

It was found that DNN1 had some difficulty with distinguishing between superconducting IV-curves and IV-curves with steps. It was decided that these curves could be most easily distinguished through an 8th-degree polynomial fit using the `scipy.optimize.curve_fit` functionality.

The eight coefficients that were returned by this polynomial fit were used as inputs in the second neural network, from now on referred to as DNN2.

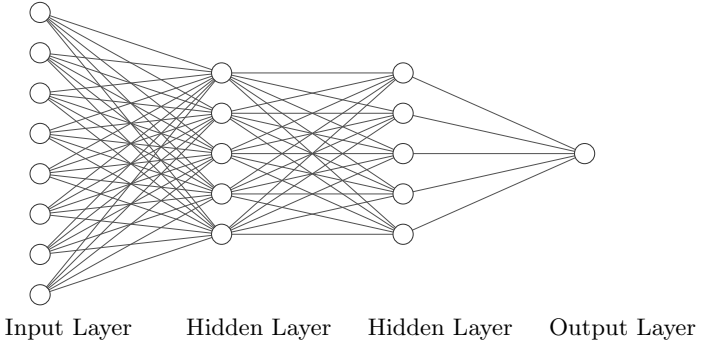


FIG. 15. Schematic of the polynomial deep neural network architecture. The input layer has eight inputs, followed by two hidden layers of five neurons each. The output layer contains one neuron. Created using [10].

At the beginning stages, it was also considering input the coefficients of an even higher curve fit polynomial. However, this would have required more time and computational resources than were available, although it might have led to an equivalent or better result.

The result of filtering a 10.000 IV-curve data set can be seen in Figure 16. The 500 curves left after DNN1/raw IV DNN mostly consisted of curves with steps and regular superconducting behaviour (for an example of this, see the orange curve in Figure 18).

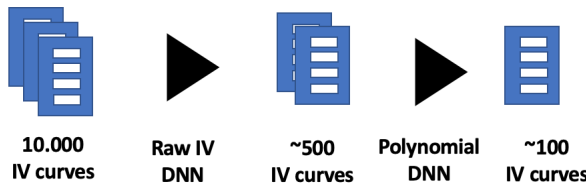


FIG. 16. This figure gives an idea of the amount data left after filtering. Amount of IV curves before filtering, after the raw IV DNN (DNN1), and after the polynomial DNN (DNN2).

B. Training Set

As mentioned previously, the machine learning architecture used requires a training set. This section will describe the criteria used in manually compiling this training set. This will be done by showing examples of graphs containing steps. For future research, the full training set is available on the project GitHub page under "lbult/SQUID_Shapiro_Practicum" > "Data" [11].

When selecting data for the two training sets, it is important there is close to no overlapping features in the IV curves. Figure 17 shows four random IV-curves from

the steps training set. As visible, these curves are distinct from regular superconducting IV-curves. The orange curve shows multiple self-defined "steps", whereas the other three show two.

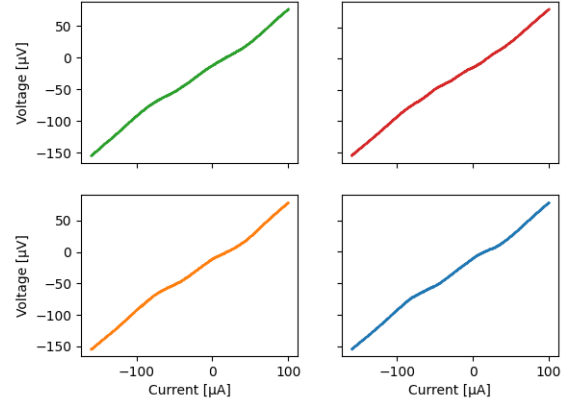


FIG. 17. Four random IV curves from the training set which the authors classified as having steps, these IV curves where used in training DNN1 and DNN2. This set can be found in "lbult/SQUID_Shapiro_Practicum" > "Data" > "Training_Shap" [11].

Figure 18 shows four random IV curves from the no steps training set. As visible, it shows three superconducting SQUID IV-curves, and one straight line. The straight line in this case is the result of an upper range RF transmitter power, with arbitrary RF frequency.

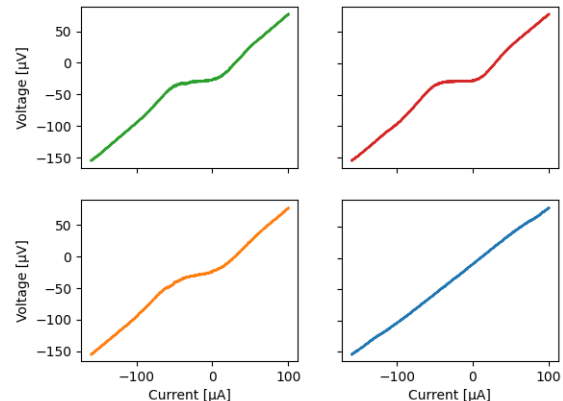


FIG. 18. Four random IV curves which the authors classified as having no steps, these IV curves where used in training DNN1 and DNN2. This set can be found in "lbult/SQUID_Shapiro_Practicum" > "Data" > "Training_NotShap" [11].

C. Training Performance

Multiple neural networks were trained using a variety of training sets, and performance varied a lot depending on the training set. Performance on the current training and verification set are shown in Table I for the different models available in the project GitHub under "lbult/SQUID_Shapiro_Practicum" > "Models" [11]. These models show some variability in performance, since their individual training sets, not the current, final version, were altered to improve performance. Additionally, it can be noticed that the DNN2, with polynomial inputs, has overall good performance. This is thought to be because of the inherent difference in polynomial coefficient for graphs with and without steps.

TABLE I. Performance in percentage correctly classified of the training neural network models. Models available in [11] under "lbult/SQUID_Shapiro_Practicum" > "Models". Training and verification set available under "lbult/SQUID_Shapiro.Practicum" > "Data". The verification set has five data points.

Model Name	Performance Training Set [%]	Performance Verification Set [%]
raw_IV_model_v1	59.6	20
raw_IV_model_v2	83.7	40
raw_IV_model_v3	87.9	80
raw_IV_model_v4	96.6	100
poly_model_v1	89.9	100
poly_model_v2	92.4	100
poly_model_v3	86.1	100
poly_model_v4	91.1	100

D. Neural Network Filtering Architecture: Shapiro Steps

Note: this section shortly outlines the neural network architecture used in detecting Shapiro steps. This work was done after the meeting on the 14th of January, and due to a lack of time left the method could not be fully worked out. Additionally, the data was very noisy, leading to sub-optimal performance of the DNN and subsequent data analysis.

Shapiro step candidates were selected using one deep neural network, from now on referred to as DNN3. This DNN, like the ones previously mentioned in Section IV A are made and trained using "MLPClassifier" function in the scikit-learn Python library [9]. The data input consisted of 330 points between 0 and 30 μ A, if there were more than 330 points in this range, data points after index 330 were cut. The output, as previously, is 1 if Shapiro steps were inferred, and 0 if no Shapiro steps were inferred. The hidden layer size was set to 175, which was chosen being around the average of the input and output layer. A schematic of the neural network

architecture can be seen in Figure 19.

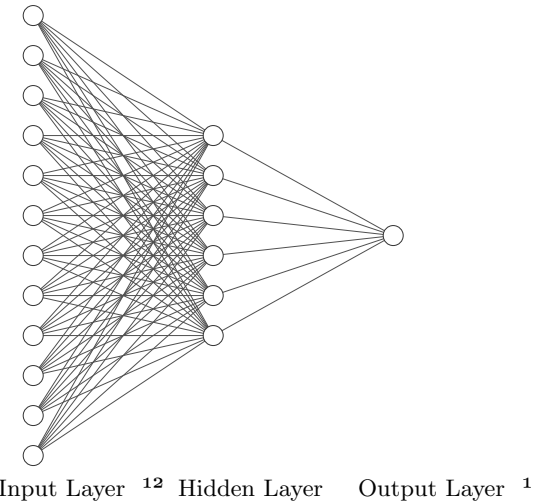


FIG. 19. Schematic of the raw IV curve deep neural network architecture. The input layer has 330 nodes, the hidden layer has 175 nodes, the output layer consists of one node.. Created using [10].

Preparing the data for train or filter input took the most time. It should also be noted that the data set is not eminently suited for the purpose of finding Shapiro steps. The IV sweeps were performed over a too large range, leading to a decreased resolution in the selected current range.

The neural network used a manually compiled data set of training examples. Random samples from the Shapiro step data set can be seen in Figure 20, those from the not Shapiro data set can be seen in Figure 21. As visible in Figure 20, multiple steps are visible in each graph. Additionally, the graphs should have the smallest possible amounts of noise.

As visible in Figure 21, training examples not containing Shapiro steps have straight line segments, are noisy, and contain large drops. As previously mentioned, the data is quite noisy. Therefore it could be that Shapiro steps are visible, but not of high enough quality for further analysis or plotting.

Since the training data only consisted of data points between 0 and 30 μ A, it is likely that other segments of the IV curve do not conform to training set requirements. However it was not possible to create a more refined method with the time resources available.

Training performance of the trained model was also briefly evaluated. The model, available via "lbult/SQUID_Shapiro_Practicum" > "Models" [11], correctly classified 100% of the training set, and 80% of the verification set (20 random samples).

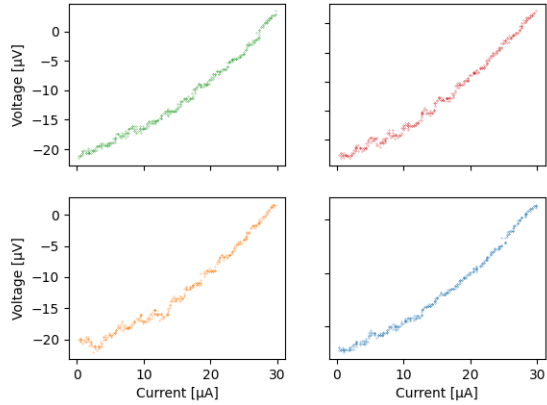


FIG. 20. Four random IV curves to show what the authors classified as Shapiro steps, these IV curves were used to train DNN3. This set can be found in "lbult/SQUID_Shapiro_Practicum" > "Data" > "Train_Shap" [11].

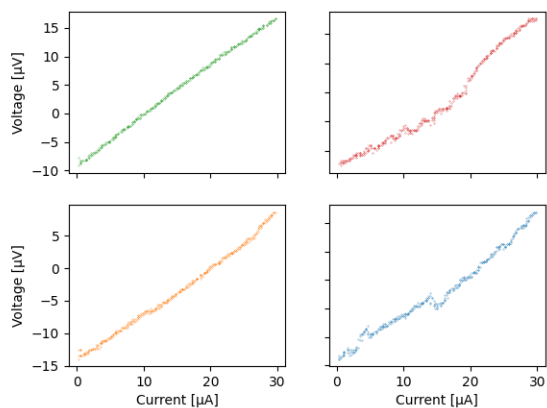


FIG. 21. Four random IV curves to show what the authors classified as no Shapiro steps, these IV curves were used to train DNN3. This set can be found in "lbult/SQUID_Shapiro_Practicum" > "Data" > "Train_NotShap" [11].

V. RESULTS AND DISCUSSION: MACHINE LEARNING METHOD

A. Observed Steps

Note: neural network performance was evaluated in the results and discussion section using steps data (i.e. steps that are not Shapiro steps) due to a lack of time after the meeting on the 14th of January.

There were two steps in analysing the performance of the deep neural networks (DNN's) on the collected data. The first step was to verify that the filtered IV curves indeed contained steps, the second to see if there was any

pattern or bias in the DNN filtered. Both can be analysed by having a look at three types of graphs. The authors will show step-by-step how conclusions were drawn out of Figures 22, 23, 24, 25, and 26.

Firstly, the RF frequency and power were noted down for each selected IV curve. These noted data points were plotted in the histogram in Figure 22 for frequencies ranging between 1000 and 3000 MHz, and in Figure 23 for frequencies ranging between 3000 and 5000 MHz. Additionally, Figure 24 shows a random sample from the data points in Figure 22. Figure 25 shows a random sample from the data points in Figure 23.

Figures 22 and 23 will give an idea about the conditions under which IV-curves, like those in the training set, will occur. If the gathered combinations of RF frequencies and powers are subsequently plotted, it might be possible to extract a useful relation between the selected IV curves. Alternatively, it could reveal DNN selection bias, i.e. the DNN only selects IV curves with steps that have a certain voltage difference.

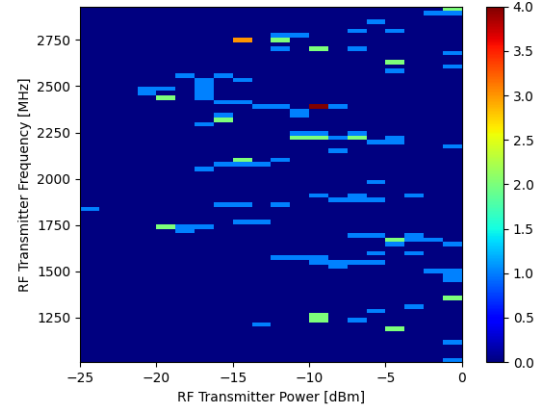


FIG. 22. Histogram of RF frequencies and powers where the neural network observed steps. Frequency range is 1000-3000 MHz, power range -25-0 dB. Colour intensity denotes the amount of detected steps in a certain histogram bin.

No clear relationship could be found between occurrence of steps, and frequency and power. Behaviour that could be vaguely observed in both Figure 22 and Figure 23 is a zigzag patter in RF transmitter power with increasing RF frequency. This will be further analysed later in this section.

Random samples of IV curves in both the range 1000 to 3000 MHz and 3000 to 5000 MHz were taken to give an idea of the IV curves selected by the DNN's. These IV curves are shown in Figure 24 for the range 1000 to 3000 MHz (and Figure 22), and Figure 25 for the range 3000 to 5000 MHz (and Figure 23).

The random samples taken from all DNN selected IV curves, shown in Figures 24 and 25, show clear similarities to those in the training set (see Figure 17). Considering the similarities, and having further looked at the

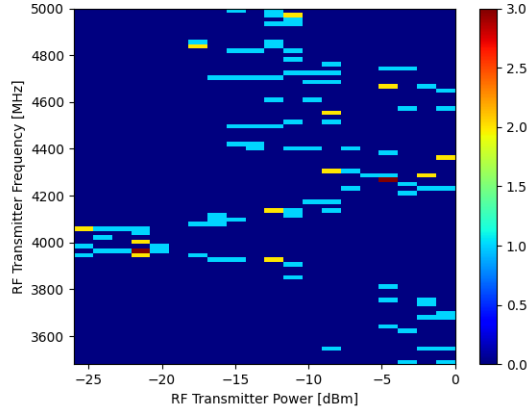


FIG. 23. Histogram of RF frequencies and powers where the neural network observed steps. Frequency range is 3600 to 5000 MHz, power range -25 to 0 dB. Colour intensity denotes the amount of detected steps in a certain histogram bin.

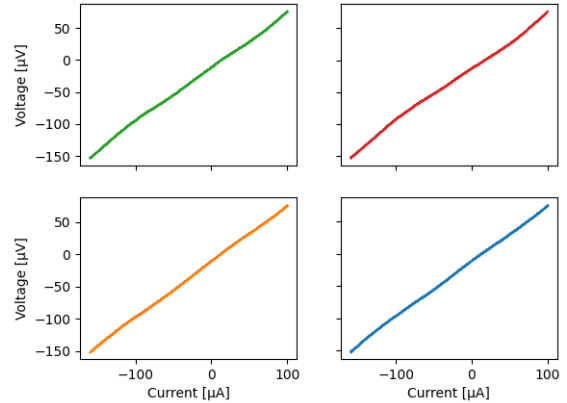


FIG. 25. Random sample of four IV-curves from the DNN selected IV-curves in the range 3000 to 5000 MHz. Similar features to those in the steps training set, visible in Figure 17, are clearly present.

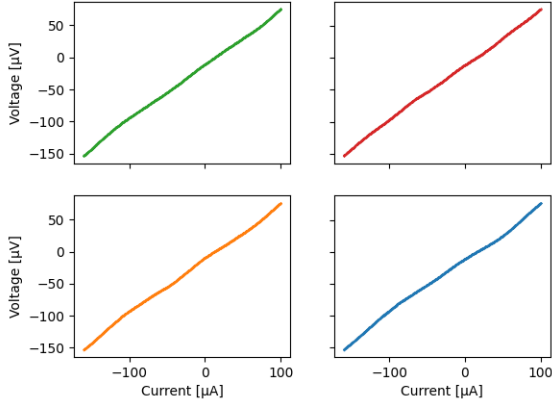


FIG. 24. Random sample of four IV curves from the DNN selected IV curves in the range 1000 to 3000 MHz. Similar features to those in the steps training set, visible in Figure 17, are clearly present.

selected curves, it is concluded that the machine learning method achieved its goal. Data filtering was automated and the IV-curves returned contained the desired characteristics.

Also visible in the randomly sampled graphs in Figures 24 and 25 is the variation of step voltage. When an RF transmitter is introduced, the regular superconducting IV curve disappears gradually with increasing power. The steps start around the flat part of this superconducting IV curve, and their spacing increases with increasing power. The power at which these steps start to be visible varies with frequency. Figure 26 shows this evolution of step voltage with increasing power. When the bright yellow line starts to diverge, for some frequencies at least, steps are introduced in the IV curve. The location of this

divergence however varies with power.

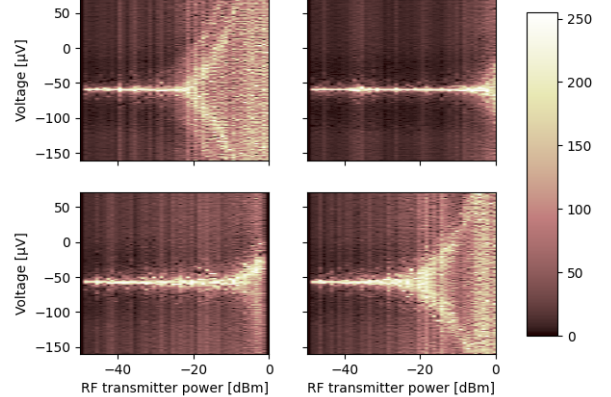


FIG. 26. Voltage histogram evolution with increasing power at four different frequencies to show evolution of this plot with increasing frequency. The top left plot is at a frequency of 2500 MHz, top right 2950 MHz, bottom left 3400 MHz, and bottom right 4500 MHz. The number of bins is 140.

Knowing that the occurrence and shape of these steps varies with power and frequency, it is possible to give at least a partial explanation of the zigzag behaviour in Figures 22 and 23. It is thought that the neural network is biased towards steps at certain voltages. Since these steps occur at different RF powers for different frequencies, the neural network is thought to detect steps corresponding to the variation of bright yellow line divergence power (see Figure 26).

One possible explanation for this behaviour was suggested by the project supervisor [8]. Constructive and destructive interference of RF waves could increase or decrease effective RF power delivered to the SQUID. Figure

27 shows a white line at the frequencies where the kinks occur. The spacing of these white lines was briefly analysed.

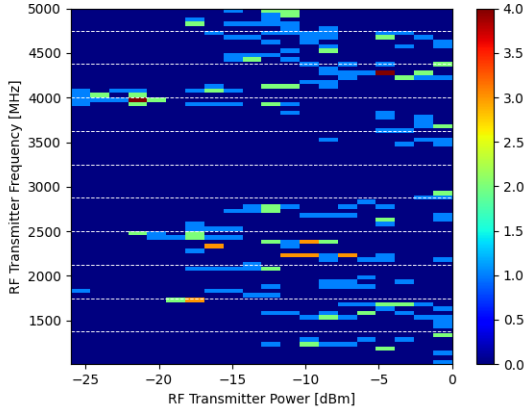


FIG. 27. Combination of Figures 22 and 23 to show periodic behaviour of kinks. The white lines have a periodicity of 375 MHz.

The graphs show that the kinks (at -25 dBm and 0 dBm) in the zigzag pattern occur at integer multiples of around 375 MHz . This means that the minimum and maximum power kinks are spaced at 750 MHz intervals, corresponding to an EM wave with wavelength 0.4 m ($\lambda = \frac{c}{f}$). This wavelength is of the same order of magnitude as the dimensions of the dewar (height 0.42 m and diameter 0.19 m). Thus, one theory is that EM waves are (partially) reflected in the container to cause constructive and destructive interference. Further research into this theorised phenomenon could lead to the possibility of using a Mr. SQUID to measure RF power through measurement of the IV curve shape or histogram.

B. Recommendations

Some ways to improve detection using the current setup would be to improve on the current training set used for the deep neural networks, leading to a reduction of falsely filtered data points. Additionally, data gathering could focus on certain regions of interest, where clear steps have previously been found. It is thought that this increased resolution might lead to better quality of detected steps, which in turn could improve the fidelity of the training neural network.

The current method used for data selection has great utility in filtering a large amount of collected data, about 90-95% of the data is (in)correctly filtered. The data left after filtering consisted almost solely of step IV curves. After exploring the selected frequencies however, it was found that some data points were misidentified with the label "no steps" (in other words false negatives). This was thought to be caused by the sometimes ambiguous

nature of graphs, caused by human interpretation and rounding of steps (see also the next paragraph).

The authors suggest exploring the use of a different machine learning architecture. It is thought that there is much performance still to gain, especially in reducing the amount of false negatives. One possibility is the use of a (deep) convolutional neural network, where matplotlib.pyplot images are used as input. It is thought that convolutional neural networks might be able to detect certain image features, which more generally are curves and straight line segments, in this case the features would be (Shapiro) steps. One possible downside to this approach however is that it is significantly more computationally expensive to train.

Lastly, to speed up the process of gathering data, the authors recommend to implement deep neural network filtering directly on the project desktop. Saving and transferring data is a time consuming process, while deep neural network inference is relatively fast. Doing this would however rely on further improvement of the data filtering method, since some Shapiro step IV-curves are also filtered out by the current model.

VI. RESULTS AND DISCUSSION: STEPS

The main goal of this chapter is to determine whether or not the observed steps are Shapiro steps. If not, maybe it is possible to say something about the behaviour of the steps.

A. Visual Inspection of Filtered Step IV curves

DNN3 selected fourteen IV curves to have (Shapiro) steps out of 1500 curves between the frequencies 4700 and 5000 MHz . These curves can be found at "lbult/SQUID_Shapiro_Pracicum" > "Data" > "Selected_Shapiro" [11]. Nearly all of those fourteen graphs contained visible steps comparable, though much noisier, to those seen in Figure 7 in [12], Figure 5 in [13], and Figure 10 in [14].

Figure 28 shows steps near the "positive" critical current, i.e. the transition area to non-superconducting behaviour when no RF generator would be present. A characteristic visible in the top-right and bottom curves is the decrease in width of the steps as the voltage and current increase, this can also be observed in the Shapiro step graphs in [12], [13], and [14].

Figure 29 shows the region around the "negative" critical current. Although some steps can be weakly identified, the data is much too noisy to learn anything useful. The discrepancy between the "negative" and "positive" critical current, and any steps that can be identified, is thought to be caused by the DNN selection around the "positive" critical current.

Figure 30 shows a wider current range, giving an insight into the center region, around a (theoretical) zero bias

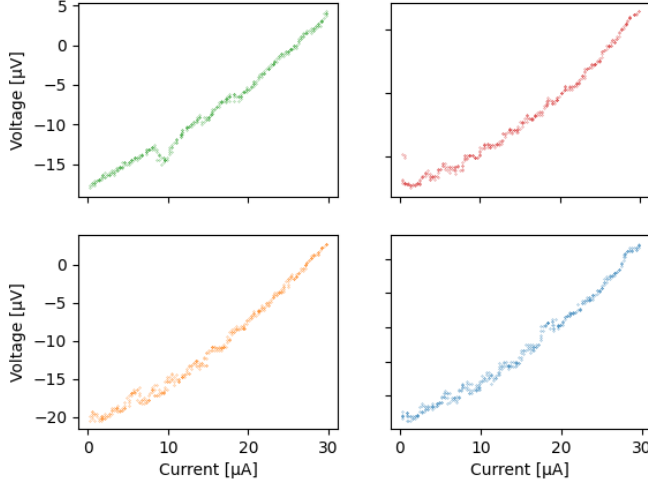


FIG. 28. "Positive" side steps of random sample of the selected IV curves. This side is used in selection of curves.

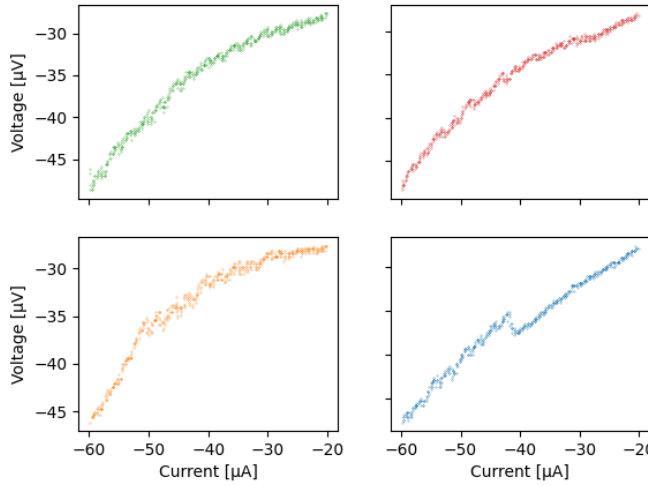


FIG. 29. "Negative" side steps of random sample of the selected IV curves. The steps can be observed, although they are very noisy.

current. Similar to the IV curves in [12] and [13] the regions show flattening around this (theoretical) zero bias current. IV-curves such as those shown in Figure 24 show a gradual transition from pure superconducting behaviour, to purely non-superconducting as RF power is increased. This is also clearly visible in Figure 30, where the different graphs also show different rates of flattening. It is concluded that although some steps are visible in the different graphs, the data is much too noisy to come to any conclusions based on visual inspection. Additionally, similarities were seen with the IV curves in [12], [13], and [14]. Thus, although nothing can yet be concluded, it is

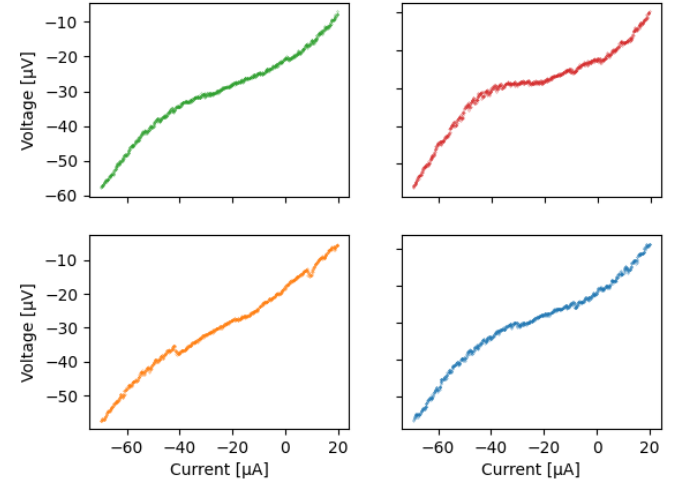


FIG. 30. "Zooming out" on the DNN3 selected IV curves to show behaviour around zero bias current.

definitely worth taking a closer look. It is recommended to probe the critical current regions more closely under RF transmission, this will likely lead to higher resolution IV curves and therefore greater insight.

B. Shapiro Step IV Curves and Histograms

To determine whether or not Shapiro steps were observed, it is necessary to look at three things. Does the step size match the theoretical step size at a given frequency, does the spacing depend linearly on frequency, and is the spacing independent of power [8]. It is thought that this can best be analysed using side-by-side IV curves and histograms at two or more RF frequencies. For both RF frequencies, the theoretical Shapiro lines were kept constant for all three RF powers.

Suggestion: it is easier to see that the IV curve steps are stationary when having the image files at disposal. By opening IV curves at the same frequency all at the same time in Windows Photos, then selecting them one by one, it is possible to see overlap in the histograms. For this purpose, the graphs in this section have been made available under "lbult/SQUID_Shapiro_Practicum" > "Photos" [11]. The graphs can be created using the Python script "analyse_steps.py" under "lbult/SQUID_Shapiro_Practicum" > "Code" > "eh_analysis".

Figures 31, 32, 33, 34, 35, and 36 show side-by-side IV curves and histograms. The histograms count the number of data points in a certain voltage bin. For a clean data set, without too much noise, the relative number of counts (with respect to other bins) gives an indication on the slope of the IV curve. A steep section would have few counts, whilst a flat section has a high number

of counts. The bin thus form an approximation for the slope of the IV curve, with the number of counts being inversely proportional to the slope. Unfortunately the data set is not perfect, and contains a lot of noise which leads to some spread of otherwise clear bin count maxima. The histograms thus form an attempt at deducing some properties.

All plots were selected as to have as little noise as possible, such that analysis could be performed. This resulted in there being RF power "gaps" between the different plots. Additionally, hand-selecting curves can lead to results which favor the researcher. Thus, although some properties were observed across multiple RF powers, it could be that some properties are due to human selection, and not inherent properties.

Plots such as Figure 3 in [15] could unfortunately not be plotted. Data alignment issues, wrong IV sweep resolution, and noise are thought to be the most likely causes. These graphs would be able to give even more insight into the observed steps, and provide another method of verifying that the steps observed were indeed Shapiro steps. It must also be noted that frequencies 3400 MHz and 4900 MHz were the first frequencies analysed with this method. Additionally they were randomly chosen, with the only criteria being that they were far enough apart to observe linear dependence of step size on frequency.

Figure 31 shows an IV curve where the RF transmitter frequency is 3400 MHz, with a power of -28 dBm. From the bottom up, theoretical Shapiro step (red dotted) lines 2, 3, 4, 5, 7, 8 seem to visually line up with a step. Additionally, red lines 2, 3, 4, 8 line up with a "local maximum" number of bin counts.

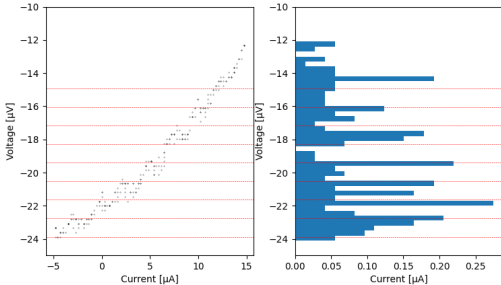


FIG. 31. IV curve of steps at an RF transmitter frequency of 3400 MHz and a power of -28 dBm. The red dotted lines denote the theoretical locations of Shapiro steps.

Figure 32 shows an IV curve where the RF transmitter frequency is 3400 MHz, with a power of -27 dBm. From the bottom up, theoretical Shapiro step (red dotted) lines 2, 3, 4, 6, 7 seem to visually line up with a step. Additionally, red lines 2, 3, 4, 7 line up with a "local maximum" number of bin counts.

Figure 33 shows an IV curve where the RF transmitter frequency is 3400 MHz, with a power of -23 dBm. From the bottom up, theoretical Shapiro step (red dotted) lines 2, 3, 4, 5, 6, 8 seem to visually line up with a step.

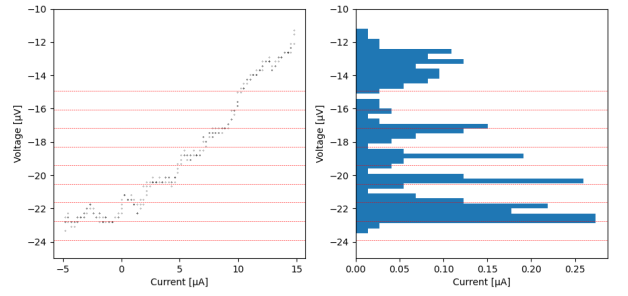


FIG. 32. IV curve of steps at an RF transmitter frequency of 3400 MHz and a power of -27 dBm. The red dotted lines denote the theoretical locations of Shapiro steps.

Additionally, red lines 1, 2, 3, 4, 5, 6, 8 line up with a "local maximum" number of bin counts.

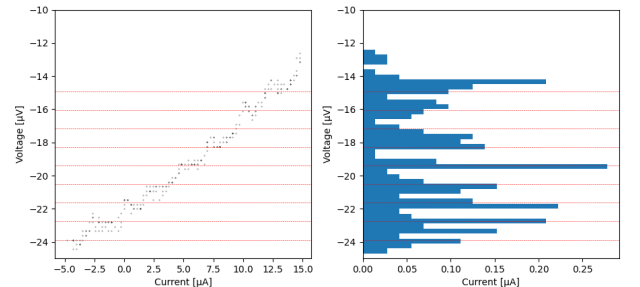


FIG. 33. IV curve of steps at an RF transmitter frequency of 3400 MHz and a power of -23 dBm. The red dotted lines denote the theoretical locations of Shapiro steps.

Combining the results of the visual inspection of Figures 31, 32, and 33, red lines 2,3,4,8 aligned with a step three times.

Figures 34 and 35 show an IV curve where the RF transmitter frequency is 4900 MHz, with a power of -27 dBm and -25 dBm respectively. From the bottom up, theoretical Shapiro step (red dotted) lines 1, 2, 3, 4, 5 seem to visually line up with a step in both the IV curve and the histogram, in both plots.

Figure 36 shows an IV curve where the RF transmitter frequency is 4900 MHz, with a power of -3 dBm. From the bottom up, theoretical Shapiro step (red dotted) lines 1, 2, 3, 4, 5 seem to visually line up with a step in both the IV curve and the histogram, in both plots. It is noted that there are more peaks than theoretically predicted Shapiro steps, and the theoretically predicted lines are slightly offset from the local maxima and steps.

Analysis of Figures 31, 32, 33, 34, 35, and 36 has shown periodicity of steps consistent with theoretically predicted Shapiro steps at four frequencies (more graphs can be found in "lbult/SQUID_Shapiro_Practicum" > "Photos" [11]). Observation of these steps is however not limited to these four frequencies, from random sampling of frequencies it seems likely that IV-curves at all RF fre-

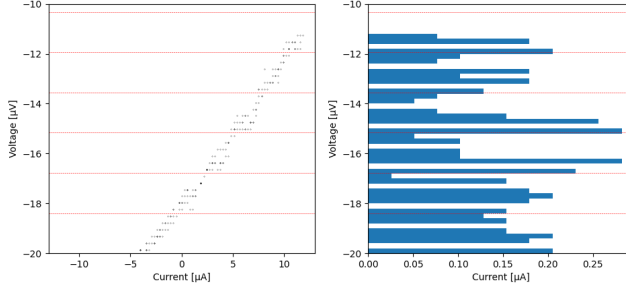


FIG. 34. IV curve of steps at an RF transmitter frequency of 4900 MHz and a power of -27 dBm. The red dotted lines denote the theoretical locations of Shapiro steps.

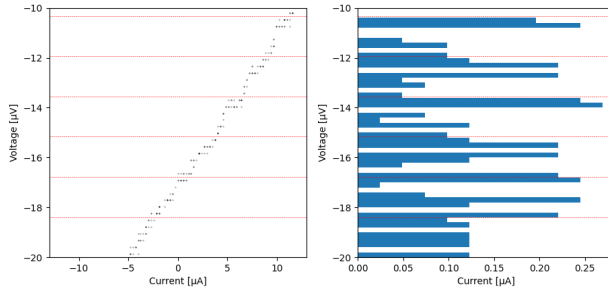


FIG. 35. IV curve of steps at an RF transmitter frequency of 4900 MHz and a power of -25 dBm. The red dotted lines denote the theoretical locations of Shapiro steps.

quencies have these steps. Additionally, constant voltage occurrence of steps has been demonstrated. It must however be noted that the test size is limited and therefore any statistically significant conclusion cannot be made. Additionally, calculation of the bin step size was not possible, due to a lack of resolution.

Concluding, the data analysed is quite noisy, the authors must therefore be cautious with making a definite statement on whether the steps that occurred were indeed Shapiro steps. However, the previous visual inspection of IV curves (in Section VIA) and in this section give some cautious optimism that indeed Shapiro steps were observed.

C. Recommendations for the confirmation of Shapiro steps

In order to determine with great certainty that the steps found are actually Shapiro steps one promising option comes to mind. This option involves making use of gaussian distributions in the histograms to determine the bin step size. The histograms will be overlaid with a mixture of gaussian distributions. The peaks of the gaussians have to line up with the theoretical Shapiro step size for a certain frequency and the histogram peaks. To make

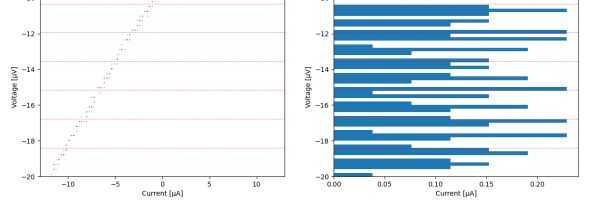


FIG. 36. IV curve of steps at an RF transmitter frequency of 4900 MHz and a power of -3 dBm. The red dotted lines denote the theoretical locations of Shapiro steps.

sure the uncertainty is very low these gaussians have to be very narrow. This application can be realized by making use of either functions of SciPy or Scikit-Learn, these are Kernel Density Estimation and Gaussian Mixture respectively. However, it is therefore necessary to use the appropriate parameter settings (such as bandwidth) and optimal bin size in the histograms. In order for any of this to work the IV sweeps need to be done over a smaller range than was used in this experiment. This is necessary to increase the resolution in the selected current range. Figure 37 shows a first impression of what such an overlayed histogram looks like with crude settings. The method used is that of the Kernel Density Estimation.

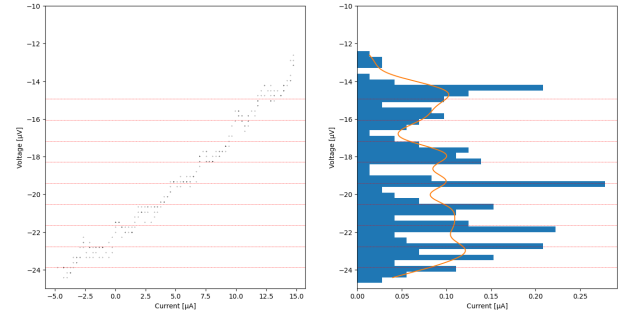


FIG. 37. Histogram with KDE overlay. $f = 3400$ MHz and $P = -23$ dBm.

Lastly, it was brought to the authors' attention that there might be other sources that could cause the observed steps. [16] Considering that no elaborate literature survey was performed during this research project, it is recommended for further research to do a broad literature survey, containing all possible sources that could cause steps similar to those observed.

VII. CONCLUSION

The machine learning method used has successfully demonstrated that it is capable of selecting IV curves similar to the ones in the training set. It provides a framework for finding Shapiro steps on any Josephson junction with microwave excitation. It is recommended to explore replacement of the current machine learning method by a different machine learning architecture, with the goal of decreasing the amount of false negatives (i.e. deletion of relevant IV curves).

IV-curves, such as those in the "New_Training_Shap" data set, were found to occur at different RF power for varying frequency. This variation was visible as a zigzag pattern in a 2D histogram. It was theorised that this zigzag pattern is the result of constructive and destructive interference of the RF transmitter electromagnetic waves. This was substantiated with the sampled RF frequencies having a wavelength in the same order of magnitude as the dimensions of the dewar. Future research could focus on using the current test setup as an RF power measurement device.

Periodicity of observed steps consistent with theoretically predicted Shapiro steps has been demonstrated at four frequencies. Constant voltage occurrence of steps at varying power has also been demonstrated. Additionally, Shapiro step candidates were visible on every sampled frequency to date. It must be noted that the test size is too small for a statistically significant conclusion. Therefore, the authors come to the conclusion that although there is some evidence to support the observation of Shapiro steps, it is left to future experimentation to confirm this observation.

To come to a definitive conclusion on whether the current experimental setup is capable of observing Shapiro steps, it is recommended to gather data with a smaller (bias) current amplitude. This is expected to increase the quality of the histogram analysis, and provide the opportunity to measure the step size of the Shapiro step

candidates. Additionally, it is recommended to do a literature survey of other possible sources that could cause the observed Shapiro step candidates.

ACKNOWLEDGEMENT

We would like to thank Professor Steele and Professor Ali for their input and guidance during this research project. Additionally we would like to thank Jasper Franse, Jean-Paul van Soest, and Heng Wu for their help with our lab work.

APPENDIX

TABLE II. List of contributions

Contributor	Experiment	Report
Bram	Experiment execution Data collection Coding analysis Data analysis	Method: Experimentation R/D: Steps Appendix Introduction Theory
Lennart	Experiment execution Data collection Coding ML Coding analysis Data analysis	Method: ML R/D: ML R/D: Steps Introduction Theory Conclusion
Nick	Experiment execution Data collection	Abstract Introduction Theory

-
- [1] Jasper Franse Gary Steele Daniel Bothner, Ines Corveira Rodrigues. Tn2953-p the josephson junction: Quantum tunnelling and interference in an electrical circuit. <https://nsweb.tn.tudelft.nl/gsteele/SQUID-practicum/TN2513-P%20SQUID%20Practicum%20Manual.html>, 2022.
- [2] M. S. Colclough G. Zaharchuk R. Cantor R. W. Simon, M. J. Burns. *Mr. SQUID® User's Guide*. Star Cryoelectronics LLC.
- [3] Star Cryoelectronics LLC. Mr squid user's guide.
- [4] Roberta Caruso. I-v curves showing shapiro steps for different microwave frequencies. https://www.researchgate.net/figure/I-V-curves-showing-Shapiro-steps-for-different-microwave-frequencies-Inset-width-of-the_fig4.325215571, 2022.
- [5] Jen-Tzong Jeng. Different dbm shapiro steps. https://www.researchgate.net/figure/Shapiro-steps-under-microwave-irradiation-with-0-2-3-5-and-7-dbm_fig7_266399846, 2022.
- [6] Star Cryoelectronics LLC. Mr. squid information. <https://starcryo.com/mr-squid/>, 2022.
- [7] Windfreak Technologies LLC. Windfreak synthnv pro specifications description. <https://windfreaktech.com/product/synthnv-pro-12-5mhz-6-4-ghz-rf-signal-generator-plus-rf-detector/>, 2022.
- [8] Prof. Gary Steele.
- [9] F. Pedregosa, G. Varoquaux, A. Gramfort, V. Michel, B. Thirion, O. Grisel, M. Blondel, P. Prettenhofer, R. Weiss, V. Dubourg, J. Vanderplas, A. Passos, D. Cournapeau, M. Brucher, M. Perrot, and E. Duchesnay. Scikit-learn: Machine learning in Python. *Journal of Ma-*

- chine Learning Research*, 12:2825–2830, 2011.
- [10] Create nn svg. Available at <http://alexlenail.me/NN-SVG/index.html>. (Date last accessed: 16 January 2022).
- [11] Lennart Bult, Bram Wagemakers, and Nick Verhoeks. Squid shapiro practicum github page. Available at https://github.com/lbult/SQUID_Shapiro\Practicum. (Date last accessed: 14 January 2022).
- [12] C. Wu, W. Kuo, J. Chen, and Jen-Tzong Jeng. A nanoscale-localized ion damage josephson junction using focused ion beam and ion implanter. *Journal of Nanoscience and Nanotechnology*, 15, 05 2015.
- [13] Tom Godfrey, J.C. Gallop, David Cox, Ed Romans, Jie Chen, and Ling Hao. Investigation of dayem bridge nanosquids made by xe focussed ion beam. *IEEE Transactions on Applied Superconductivity*, PP:1–1, 07 2018.
- [14] Leonid Rokhinson, Xinyu Liu, and Jacek Furdyna. The fractional a.c. josephson effect in a semiconductor-superconductor nanowire as a signature of majorana particles. *Nature Physics*, 8:795–799, 11 2012.
- [15] Jonas Wiedenmann, Erwann Bocquillon, R. Deacon, S. Hartinger, O. Herrmann, T.M. Klapwijk, Luis Maier, Christopher Ames, Christoph Brüne, C. Gould, Akira Oiwa, K. Ishibashi, Seigo Tarucha, H. Buhmann, and L. Molenkamp. 4-periodic josephson supercurrent in hgte-based topological josephson junctions. *Nature Communications*, 7:10303, 01 2016.
- [16] Prof. Mazhar Ali.